ACS OMEGA

Article

Cite This: ACS Omega 2019, 4, 1265−1271

http://pubs.acs.org/journal/acsodf

Induced Lanthanide Circularly Polarized Luminescence as a Probe of Protein Fibrils

Monika Krupová,[†,‡] Josef Kapitán,[§] and Petr Bouř*[,†]

[†]Institute of Organic Chemistry and Biochemistry, Academy of Sciences, Flemingovo náměstí 2, 16610 Prague, Czech Republic

[‡]Faculty of Mathematics and Physics, Charles University, Ke Karlovu 3, 12116 Prague 2, Czech Republic

[§]Department of Optics, Palacký University, 17. listopadu 12, 77146 Olomouc, Czech Republic

Supporting Information

ABSTRACT: Protein fibrils are involved in a number of biological processes. Because their structure is very complex and not completely understood, different spectroscopic methods are used to monitor different aspects of fibril structure. We have explored circularly polarized luminescence (CPL) induced in lanthanide compounds to indicate fibril growth and discriminate among fibril types. For hen egg-white lysozyme and polyglutamic acid-specific CPL, spectral patterns were obtained and could be correlated with vibrational circular dichroism (VCD) spectra and thioflavin T fluorescence. The CPL spectra were measured on a Raman optical activity spectrometer, and its various polarization modes are discussed. The experiments indicate that the induced CPL is sensitive to more local aspects of the fibril structure than VCD. For CPL, smaller amounts of the sample are required for the analysis, and thus this method appears to be a good candidate for future spectroscopic characterization of these peptide and protein aggregates.

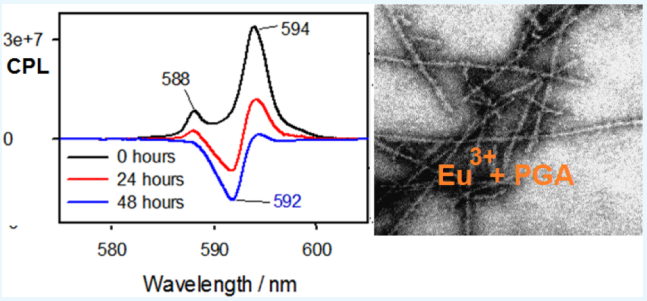

INTRODUCTION

Insoluble protein aggregates, quite often in a form of threads-fibrils, are omnipresent in human and animal biology. In medicine, they draw particular attention because of their role in a range of neurodegenerative disorders, including Alzheimer's, Parkinson's, diabetes, and prion diseases.[1] Formation and growth of the fibrils are multistep processes that are only partially understood.[2] Fibril structure is very variable depending on the conditions, and not much is known about the link to the sequence of the protein.[3,4]

As only a fraction of fibril systems can be crystallized,[5] lower-resolution spectroscopic methods have been vigorously pursued. Particularly useful are chiroptical methods, providing a relatively detailed insight into dynamics of fibril growth in solutions.[6−9] Vibrational circular dichroism (VCD) is perhaps the most sensitive spectroscopy indicating fibril formation. If compared with proteins in their native states, formed fibrils provide a huge enhancement of the signal, about 10 to 100 times larger in terms of the VCD/absorption ratio.[6,9−17] As a drawback, high concentrations are required and polarization artifacts are often observed for VCD.[9] A complementary method to VCD is Raman optical activity (ROA), potentially more suitable for the natural aqueous environment. However, it is currently not sensitive enough to provide insights into the fibril structure. Because of the light scattering and polarization effects, the ROA fibril spectra are often covered with false signals and are difficult to interpret.[18,19]

In the present study, we are testing a related chiroptical technique, circularly polarized luminescence (CPL) of lanthanide complexes induced by the chiral protein environment. As a relatively new protocol, the CPL was measured on an ROA spectrometer.[20] The technique takes advantage of optical properties of the lanthanide ions (Ln^{3+}). Their luminescence is extremely sensitive to their local chemical environment.[21,22] The strong laser excitation used in ROA makes it possible to explore weak CPL signals, often invisible otherwise. In the past, lanthanide CPL has been applied to amino acids, peptides, and saccharides, but application for fibrils is not known to us.[23−25] On the other hand, "conventional" CPL of the thioflavin T (ThT) dye absorbed on insulin fibrils did provide encouraging results.[26] Unlike the organic dyes, lanthanides provide more numerous and sharper bands, and hence potentially more information about studied systems.

Here, we explore the $EuCl_3$ and $Na_3[Eu(DPA)_3]$ compounds as luminescence "probes" of two model fibril systems. Indeed, the interaction with the protein appears to be quite specific. For example, polyglutamic acid induced large CPL signal in $EuCl_3$ that could be related to the VCD spectra and fibril maturation. On the other hand, the $EuCl_3$ gave negligible CPL for hen egg-white lysozyme (HEWL), where much larger

Received: November 14, 2018
Accepted: December 27, 2018
Published: January 15, 2019

DOI: 10.1021/acsomega.8b03175
ACS Omega 2019, 4, 1265−1271

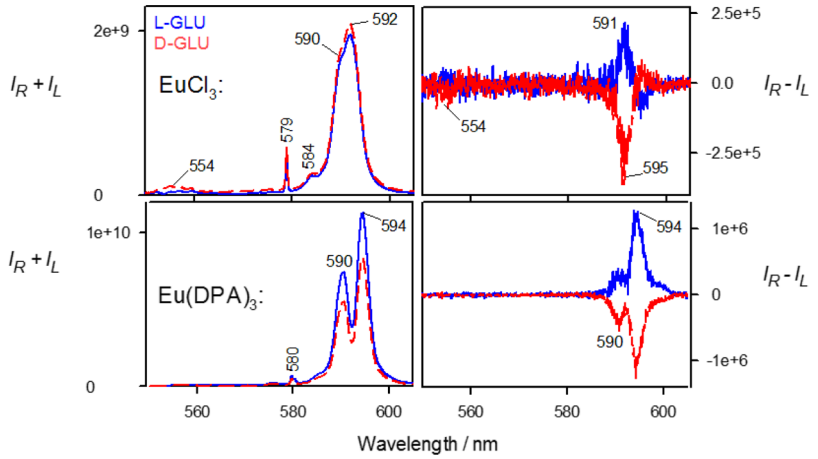

Figure 1. TL and CPL spectra of (monomeric) D- and L-glutamic acid (15 mM) and $EuCl_3/Na_3[Eu(DPA)_3]$ (top/bottom, both 5 mM).

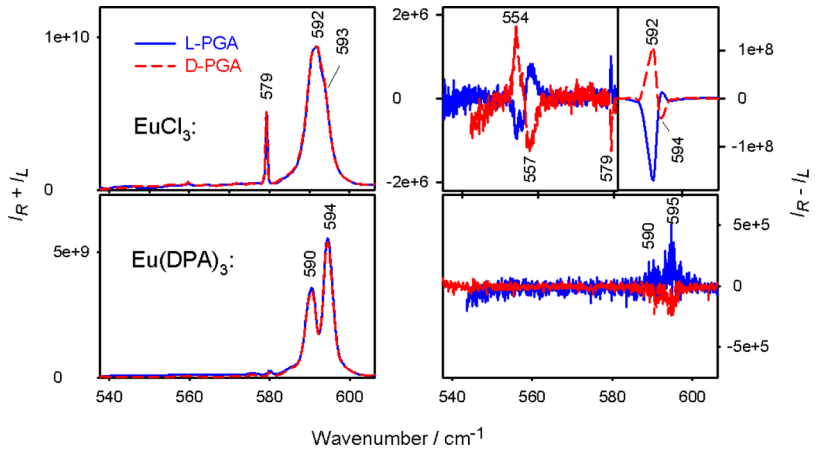

Figure 2. TL (left) and CPL (right) spectra of D- and L-polyglutamic acid with $EuCl_3$ (top) and $Na_3[Eu(DPA)_3]$ (bottom, both 1 mM), after 48 h of fibril incubation. D- and L-PGA concentrations were 10 mg/mL in H_2O, pH regulated by HCl to 4.3, the incubation proceeded at 60 °C.

CPL was obtained with $Na_3[Eu(DPA)_3]$. The spectral intensities and signs can thus be related to the protein and fibril structure. We believe that such results indicate the enormous potential of the combined ROA/CPL technique for future fibril studies, including imaging in living cells.

The manuscript is organized in such a way that we first document the properties and involved transitions of europium(III) total luminescence (TL) and CPL for (monomeric) glutamic acid and then investigate induced CPL for fibrils grown from polyglutamic acid and HEWL solutions. The fibril spectra are compared with VCD and ThT fluorescence, as these two methodologies are established as reliable fibril indicators before.[27] Finally, different ROA spectrometer polarization modes and an extended wavelength range are shown to document possibilities of the CPL/ROA method and reveal some physics of the induced chirality phenomenon.

RESULTS AND DISCUSSION

Interaction of Europium Probes with Glutamic Acid. As the simplest case documenting induced Eu^{3+} chirality and involved transitions, the $EuCl_3$ and $Na_3[Eu(DPA)_3]$ reagents were mixed with (monomeric) D- and L-glutamic acid solutions (Figure 1). Conventionally, lanthanide electronic levels are characterized using the atomic spectroscopic symbols, although the levels can split and transition bands become broader in molecules and crystals.[21,22] For $EuCl_3$ (upper part of the figure), we can see two strong TL bands of Eu^{3+}: a narrow $^5D_0 \rightarrow {}^7F_0$ peak at 579 nm and a broad $^5D_0 \rightarrow {}^7F_1$ transition band around 590−592 nm.[24,25] The $^5D_0 \rightarrow {}^7F_0$ transition does not give measurable CPL, but $^5D_0 \rightarrow {}^7F_1$ provides a positive peak at 591 nm and a smaller negative one at 595 nm (the signs relate to the L-enantiomer). A very weak positive CPL band occurs around 554 cm^{-1}, assignable to $^5D_1 \rightarrow {}^7F_2$.[24,25] Its TL is weak as well, nearly hidden in the background. Maximal CPL/TL ratio (given as the dimensionless circular intensity difference, CID, usual in the ROA spectroscopy[28]) is about 10^{-4}. Such a relatively small value indicates a weak nonspecific interaction between the europium ion and the acid, that is, only a small portion of the glutamic acid molecules directly interacts with Eu^{3+}.[24,25] In a case of strong coordination/covalent binding between europium probes and chiral ligands[29] or for rigid chiral complexes,[20,30] much higher CIDs are possible, up to the order of one. This is clearly not the case here.

Maximal TL of the $Na_3[Eu(DPA)_3]$ complex (Figure 1, bottom) is about 4.5-times bigger than for $EuCl_3$, and splitting of the main $^5D_0 \rightarrow {}^7F_1$ band is more visible as the bands at 590 and 594 nm. The $^5D_0 \rightarrow {}^7F_0$ band is somewhat split and its maximum slightly shifted to 580 nm. Also, CPL induced in the $[Eu(DPA)_3]^{3-}$ ion by the glutamic acid is different from that for $EuCl_3$, dominated by two strong $^5D_0 \rightarrow {}^7F_1$ (positive for L-

DOI: 10.1021/acsomega.8b03175
ACS Omega 2019, 4, 1265−1271

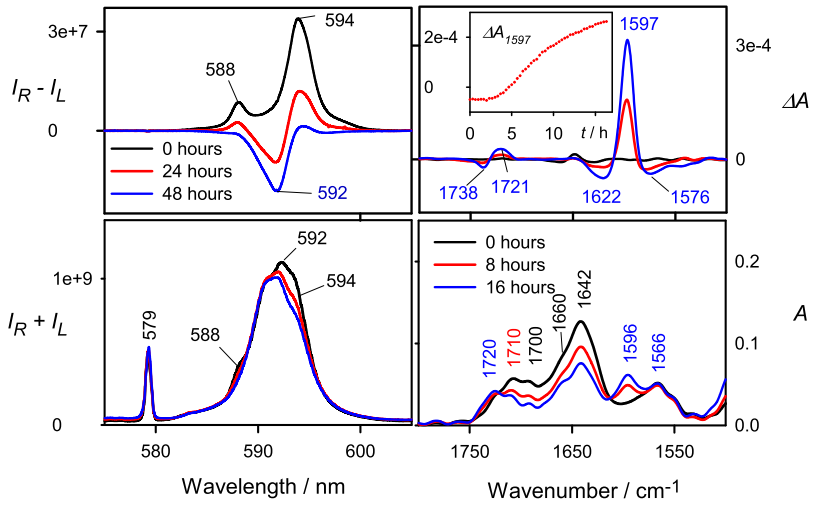

Figure 3. L-PGA fibrils, TL, and induced CPL of the $EuCl_3$ probe (left) and VCD and IR spectra (right) recorded during the fibril growth and maturation. In the inset graph, typical kinetics of the fibril growth is documented on the dependence of VCD intensity at 1597 cm^{-1} on time. pH was regulated by HCl to 4.3, incubation at 60 °C, for CPL (left) L-PGA concentration was 10 mg/mL in H_2O. For VCD (right), D_2O was used under the same conditions as for CPL, the VCD measurement proceeded in BaF_2 windows with 50 μm spacer.

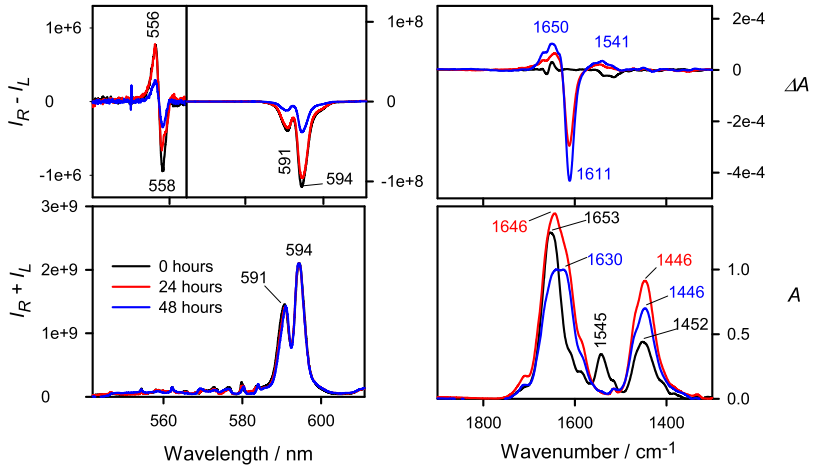

Figure 4. (Left) CPL and TL/Raman spectra of $Na_3[Eu(DPA)_3]$ and HEWL, and (right) VCD and IR spectra of HEWL in different stages of fibril formation. pH was regulated by HCl to 2.0, incubation proceeded at 60 °C, for CPL (left) HEWL concentration was 100 mg/mL in H_2O. For VCD (right), D_2O was used under the same conditions as those for CPL and the VCD measurement proceeded in BaF_2 windows with 50 μm spacer The 1545 cm^{-1} amide II IR band (right, bottom, at 0 h) comes from nonexchanged protons in the native protein.

Glu) bands at 590 and 594 nm. Maximal CID is about 10^{-4}, similarly as for the previous case.

Polymeric Glutamic Acid and Fibril Growth. Compared with the monomeric glutamic acid, PGA fibrils affect luminescence of the europium probes in a different way. TL spectra (Figure 2, left) exhibit minor changes only including small band shifts and relative intensity variations. However, CPL intensity of the $EuCl_3$ complex dramatically increases. Within the $^5D_0 \rightarrow {}^7F_1$ transition region, negative (592 nm) and positive (594 nm) bands appear for L-PGA, with maximum CID of 1.1×10^{-2} indicating a strong binding between the peptide and Eu^{3+}.[23] Weaker bands are apparent at 579 and around 555 nm. D- and L-PGA provide approximately "mirror image" CPL spectra; although the magnitudes are slightly different and the D-PGA fibrils grew much faster than those of L-PGA (cf. also Figure S1, Supporting Information). This is a normal behavior for poly-dispersion samples, slightly differing in composition for the two enantiomeric forms.[14]

The $Na_3[Eu(DPA)_3]$ probe gives for PGA a weak CPL (CID of 5×10^{-5}), very similar to that observed for the monomer acid. This can be understood on the basis of different natures of the europium compounds: while the positive Eu^{3+} ion of $EuCl_3$ may be well captured by the PGA carboxyl side chains, the negative $[Eu(DPA)_3]^{3-}$ ion is repelled.

Time Dependence and Fibril Growth. In Figure 3, left, TL, and CPL spectra of $EuCl_3$ in the presence of L-PGA fibrils are shown as measured at 0, 24, and 48 h from the beginning of the incubation. Already at $t = 0$ h, a strong positive (for the L-form) CPL signal appears, with a maximum at 594 nm. This indicates that unlike for the monomer glutamic acid PGA side chains cooperate in capturing the Eu^{3+} ion. The induced CPL is in addition dependent on PGA conformation and the longer-range order developing during the fibril maturation. The relatively slow convergence of the spectra in time can also be attributed to the very tight binding between PGA peptide chains, observed in fibril crystals.[31,32] The creation of

DOI: 10.1021/acsomega.8b03175
ACS Omega 2019, 4, 1265−1271

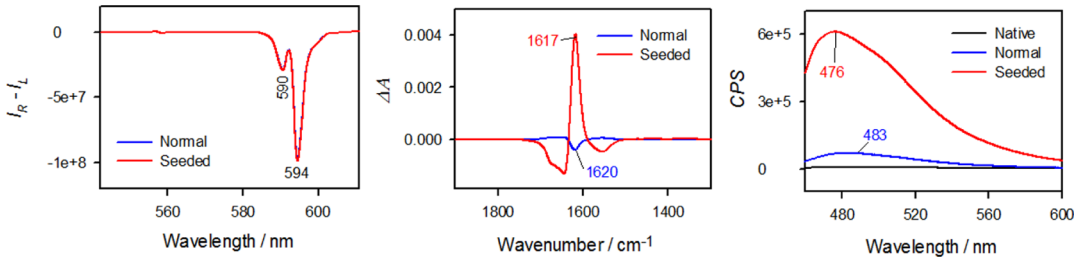

Figure 5. Comparison of the two HEWL fibril types ("normal" and "seeded", see the text) as indicated by $Na_3[Eu(DPA)_3]$ CPL (left), VCD (middle, in H_2O, 6 μm CaF_2 cell), and ThT fluorescence (right). The protein concentration was 100 mg/mL (0.5 mg/mL for ThT), in H_2O, pH was regulated by HCl to 2.0, incubation proceeded 48 h at 60 °C.

bifurcated hydrogen bonds and interdigitization of the side chains is a slow cooperative process, reflected in the development of the induced CPL signal.

VCD and IR spectra (Figure 3, right) confirm the link between the CPL signal and fibril maturation. Note that detailed analysis of the PGA IR and VCD spectra can be found in previous works.[14,17,31−33] Judging from the spectral intensities, the fibrils grow faster than those in the CPL experiment, which is attributed to an effect of BaF_2 windows[34] and elevated temperature (~30 °C), currently impossible to control in the VCD instrument. As expected, the VCD signal of fresh PGA solution (t = 0 h) is very weak. After a latent stage, it quickly rises and adopts VCD shape characteristic for fibrils (cf. also the inset graph with the time dependence of the 1597 cm^{-1} VCD intensity). The enhancement mostly occurs for the amide I vibrations (~1550−1680 cm^{-1}) and is exhibited by many proteins.[6,13,35] PGA fibrils exhibit additional enhanced VCD signal around 1730 cm^{-1} because of the carboxyl C═O stretching vibrations of the COOD side chain.[14,15,17] Relatively minor changes occur at the IR spectra, except for the 1596 cm^{-1} band absent in the native protein. This band has been previously assigned to amide I′ vibration and appears because of the fibril formation.[14] The main amide I band centered at 1642 cm^{-1} exhibits a shoulder at 1660 cm^{-1} all the time, which suggests that at least part of PGA molecules is present at the β-sheet conformation already at t = 0. This feature is only slightly more pronounced when the fibrils are formed.

Interaction of Europium with HEWL and Fibril Structure Variation. Unlike for PGA, $EuCl_3$ does not provide a measurable CPL with HEWL. Also, the weak TL of europium ion is hidden in Raman signal of the protein and background scattering (Figure S2). This can be explained by a high content of basic positively charged residues in HEWL (six lysines, one histidine, and nine arginines),[36] unable to bind the Eu^{3+} ion at low pH needed for fibril stability. On the contrary, the $[Eu(DPA)_3]^{3-}$ anion interacts with HEWL and produces strong CPL (Figure 4, left). The spectral shape, however, is less dependent on time than for PGA. Two negative bands (591 and 594 nm) are visible in the $^5D_0 \rightarrow {}^7F_1$ region, and a couplet $^5D_1 \rightarrow {}^7F_2$ appears around 557 nm. TL of $[Eu(DPA)_3]^{3-}$ is also strong and does not change. As for PGA, the presence of the fibrils can be verified by the IR and VCD spectra plotted in Figure 4, right. Also here, VCD intensity of fibrils is very much enhanced if compared with the native protein, with a dominant negative band at 1611 cm^{-1}.

The CPL intensity at 48 h appears very low compared with earlier times; however, this can be due to the large scattering of mature fibrils. Because also the CPL band shapes do not change much in time, we may conclude that HEWL induced Eu CPL is less sensitive to fibril growth/maturation than that of PGA and also than that of HEWL VCD. This is likely caused by the different structure of the fibrils and "short-sightedness" of the $[Eu(DPA)_3]^{3-}$ probe. While PGA fibrils are crystal-like and quite compact,[31,32] HEWL ones are likely to resemble more common thread-like structures.[3,4,11]

To obtain further insights into the HEWL—$Na_3[Eu(DPA)_3]$ interaction, we measured induced CPL at two pH values and different HEWL/$Na_3[Eu(DPA)_3]$ molar ratios ("Job's plots[37]") and its dependence on $Na_3[Eu(DPA)_3]$ concentration. Resultant dependencies (Figure S3) consistently indicate that one HEWL molecule binds on average about 1.5 $[Eu(DPA)_3]^{3-}$ ions at pH 7 and 3 ions at pH 2, confirming thus the importance of protein charge for the interaction. Nevertheless, we realize that the single-site binding model is only approximate, and actual interaction between the protein and lanthanide probe is more complicated. This is also indicated by the deviation of the slopes in the Job's plots from linearity. The extent of variation of the protein electrostatic potential caused by the pH change and regulating the $[Eu(DPA)_3]^{3-}$/HEWL binding is illustrated in Figure S4.

Polymorphism of HEWL Fibrils. Similarly as for other proteins and peptides,[9,11,13] HEWL fibrils exist in polymorphic forms. In aqueous (D_2O) solutions of the natural protein, the fibrils grow slowly and provide moderately enhanced VCD with a strong amide I negative band. When the solution, however, is "seeded" with pregrown fibrils, the growth is much faster, the enhancement is bigger, and the sign of the most intense peak flips. Because the VCD enhancement is supposed to reflect long-range order of the amide chromophores,[35] we may interpret this as that the seeds make larger protein aggregates easier by a catalytic effect. As follows from the comparison of the induced Eu CPL, VCD, and ThT fluorescence (Figure 5), the VCD technique is the most sensitive to such fibril morphology differences, where the "seeded" fibrils provided a huge positive band at 1617 cm^{-1}. The flip of VCD sign indicates that the two fibril types may mainly differ in a long-order twist.[6,11,35] Also, the ThT dye provides about 8 times larger fluorescence, whereas CPL is rather indifferent, with negligible changes of main peak frequencies. This confirms the observation that the $[Eu(DPA)_3]^{3-}$ ion is sensitive only to the environment in the vicinity of the metal ion; the protein mainly disturbs the equilibrium between the Δ and Λ enantiomeric forms $[Eu(DPA)_3]^{3-}$.[23] On the other hand, longer fibrils enable long-range coupling of the amide chromophores which most probably leads to the VCD enhancement.[35,38] The VCD technique is thus more sensitive to the longer-range structure ordering than the induced CPL. The change in ThT

DOI: 10.1021/acsomega.8b03175
ACS Omega 2019, 4, 1265−1271

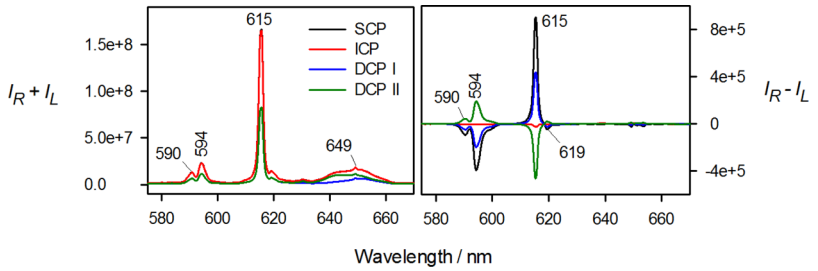

Figure 6. TL and CPL spectra of the $[Eu(DPA)_3]^{3-}$ ion in presence of HEWL fibrils recorded in various polarization modes (SCP, DCP_I, DCP_{II}, and ICP, see Figure S5 and text). The protein concentration was 100 mg/mL in H_2O, pH was regulated by HCl to 2.0, incubation proceeded 48 h at 60 °C, spectra collection times were about 10 min.

fluorescence may be related to local concentration and other factors related to longer-range interactions.[27]

Other ROA Modulation Schemes. In addition to the scatter circular polarization (SCP), the custom-built ROA spectrometer enables one to record other polarized spectra (Figure S5).[20,39] They show versatility of the method and cast some light on the mechanism of chirality induction in the lanthanide probes. This is documented for TL and CPL of the HEWL/$[Eu(DPA)_3]^{3-}$ mixture in Figure 6. A wider interval of wavelengths could be recorded, including the $^5D_0 \rightarrow {}^7F_2$ band around 615 nm. The SCP regime where the sample is irradiated with unpolarized light provides the usual CPL spectrum. During the DCP_I and DCP_{II} modulations, the sample is irradiated with circularly polarized light, and resultant spectra in principle also reflect different absorption (circular dichroism) of the left- and right-circular polarization. In our case, this seems to be negligible, and the spectra can be related to the CPL signal, too, as $DCP_I \approx CPL/2$ and $DCP_{II} \approx -CPL/2$. The initial polarization effect is nearly "lost" during the energy transfer because of the long (~1 μs) state lifetimes.[24] For this system, only the ICP mode thus provides additional information to SCP. Here, the induced chirality comes primarily from the small difference in absorption of the left- and right-circularly polarized excitation radiation. The ICP spectrum is thus formally equal to fluorescence-detected circular dichroism (FD CD).[40−42] Indeed, only the ICP curve in Figure 6 is readily different and the intensity is much smaller than that for the other experiments.

Within the reviewing process of the present study, an interesting question rose about the advantages of such ICP measurements against conventional FD CD or CD instruments. Using the ROA/CPL method, current restriction to one excitation (532 nm) is certainly a serious limitation, although instruments using other excitation wavelength start to appear as well.[43−45] On the other hand, the strong laser excitation used in ROA instruments allows one to detect even weak fluorescence bands, undetectable otherwise.[25]

CONCLUSION

We have explored the combined ROA/CPL technique and induced CPL in the europium $EuCl_3$ and $Na_3[Eu(DPA)_3]$ "probes" for indication of fibril formation, growth, and structure. The $EuCl_3$ salt was found applicable for polyglutamic acid fibrils, where the induced CPL spectra were strong. In addition, spectral shapes changed in fibril maturation stages, similarly as for the standard VCD technique. For the HEWL, the $Na_3[Eu(DPA)_3]$ complex provided more usable CPL than $EuCl_3$, and the spectral shape was somewhat less sensitive to fibril maturation. The $[Eu(DPA)_3]^{3-}$ ion also provided nearly the same CPL spectra for two fibril types.

The induced CPL is thus primarily sensitive to the local metal environment and parts of the protein/peptide directly interacting with the europium compounds. On the other hand, VCD and ThT fluorescence reflect also longer-range ordering. Therefore, these different spectroscopic techniques appear complementary in that they sample different aspects of the fibril geometry.

CPL/ROA spectra obtained with different polarization modulations provided insights into the induced chirality. For example, it revealed that different circular polarization of the incident radiation has a minor effect on the CPL (SCP) spectra.

On the basis of these encouraging results, we believe that the technique can become a useful tool to study fibril formation, structure, and interactions.

EXPERIMENTAL SECTION

Fibril Preparation. HEWL, L-, and D-polyglutamic acid (L-PGA, D-PGA, molecular weight ~15−50 kDa) were obtained from Sigma-Aldrich. Previously described protocols were followed.[10,14,46] For HEWL, the fibrils were grown from 10% water solution, pH was adjusted to 2.0 by HCl at 60 °C for 48 h. Alternatively, 900 μL of freshly prepared HEWL solution was mixed with 100 μL of solution containing already grown fibrils. In the latter case, the mature fibrils functioned as "seeds" and sped up the growth, providing, however, a different fibril type. For PGA, 1% aqueous solutions at pH 4.3 (HCl) were prepared and incubated at 60 °C for 96 h. To avoid water signal in the vibrational region of interest (1500−1800 cm^{-1}) for VCD and absorption (IR) measurement, the proteins were repeatedly dissolved in D_2O and lyophilized. D_2O was also used for the sample preparation; otherwise the same protocols were kept as for H_2O.

Spectra Measurement and Fibril Characterization. During the fibril growth, samples were taken at 0, 24, and 48 h and mixed with $EuCl_3$ or $Na_3[Eu(DPA)_3]$ (DPA = pyridine-2,6-dicarboxylic acid) aqueous solutions, final concentration of the europium compounds was 1 mM. CPL and TL spectra were measured on a ROA instrument ChiralRAMAN-2x (Biotools), using 532 nm laser excitation, 200 mW laser power, and about 20 min acquisition. Note that ROA is defined as $I_R - I_L$,[47,48] as opposed to the usual definition of CPL ($I_L - I_R$), where I_R and I_L are intensities of right and left circularly polarized light. Because the CPL data were recorded at the ROA spectrometer and various modulation schemes were explored, we used the definition $I_R - I_L$ even for CPL. Similarly, we use the CID = $(I_R - I_L)/(I_R + I_L)$ parameter as a

DOI: 10.1021/acsomega.8b03175
ACS Omega 2019, 4, 1265−1271

measure of relative CPL intensity, which is common for ROA. For CPL, the dissymmetry factor (g) is usually used instead, $g = 2(I_L - I_R)/(I_R + I_L)$, that is CID = $-g/2$. Measurements with different polarization schemes were done on a ROA instrument developed at Palacký University, Olomouc, according to the design of Hug[47,49] and Nafie.[39] For the spectra comparison, minor intensity adjustments were done to normalize the TL/Raman signal to the same conditions.

For IR and VCD, samples were taken at 0, 24, and 48 h of the incubation, and the spectra were measured on a ChiralIR instrument (Biotools), using BaF_2 windows and 50 μm optical pathlength, 8 cm^{-1} resolution, and 50 blocks of 2048 scans (~17 h accumulation time). D_2O spectra were subtracted as a baseline. Some samples were measured using 6 μm CaF_2 cell and H_2O as a solvent, which led only to minor changes in the fibril spectra within the amide I region.

Fluorescence measurements were realized on a FluoroMax-4 spectrometer (Horiba). Five microliters of native protein or fibril solution was added to 1 mL of 50 μM ThT solution, excitation wavelength of 440 nm, 5 nm slid width, and 5 and 0.2 nm increments were used. Baseline of the ThT stock solution was subtracted from the sample spectra.

Formation of the fibrils was also verified by the transmission electron microscopy (TEM) imaging. The solutions of mature amyloid fibrils were diluted 100× maintaining pH 2.0 for HEWL and pH 4.3 for L-PGA, then 10 μL were deposited on a carbon-coated grid and then stained with 4 wt % phosphotungstic acid. The TEM experiment was performed with a JEOL JEM-1200EX microscope.

■ ASSOCIATED CONTENT

Supporting Information

The Supporting Information is available free of charge on the ACS Publications website at DOI: 10.1021/acsomega.8b03175.

Additional spectra, HEWL/$Na_3[Eu(DPA)_3]$ titration data, description of modulation schemes, and TEM images (PDF)

■ AUTHOR INFORMATION

Corresponding Author

*E-mail: bour@uochb.cas.cz (P.B.).

ORCID

Petr Bouř: 0000-0001-8469-1686

Notes

The authors declare no competing financial interest.

■ ACKNOWLEDGMENTS

This work was supported by the Czech Science Foundation (18-05770S), Ministry of Education (LTC17012/CA15214 and CZ.02.1.01/0.0/0.0/16_019/0000729), and the Technology Agency of the Czech Republic (TE01020229).

■ REFERENCES

(1) Eisele, Y. S.; Monteiro, C.; Fearns, C.; Encalada, S. E.; Wiseman, R. L.; Powers, E. T.; Kelly, J. W. Targeting protein aggregation for the treatment of degenerative diseases. *Nat. Rev. Drug Discovery* **2015**, *14*, 759.

(2) Chatani, E.; Yamamoto, N. Recent progress on understanding the mechanisms of amyloid nucleation. *Biophys. Rev.* **2017**, *10*, 527−534.

(3) Ivanova, M. I.; Sievers, S. A.; Sawaya, M. R.; Wall, J. S.; Eisenberg, D. Molecular basis for insulin fibril assembly. *Proc. Natl. Acad. Sci. U.S.A.* **2009**, *106*, 18990−18995.

(4) Stroud, J. C.; Liu, C.; Teng, P. K.; Eisenberg, D. Toxic fibrillar oligomers of amyloid-β have cross-β structure. *Proc. Natl. Acad. Sci. U.S.A.* **2012**, *109*, 7717−7722.

(5) Eisenberg, D. S.; Sawaya, M. R. Implications for Alzheimer's disease of an atomic resolution structure of amyloid-β(1−42) fibrils. *Proc. Natl. Acad. Sci. U.S.A.* **2016**, *113*, 9398−9400.

(6) Kurouski, D.; Dukor, R. K.; Lu, X.; Nafie, L. A.; Lednev, I. K. Spontaneous inter-conversion of insulin fibril chirality. *Chem. Commun.* **2012**, *48*, 2837−2839.

(7) Nafie, L. *Vibrational Optical Activity: Principles and Applications*; Wiley: Chichester, 2011.

(8) Berova, N.; Polavarapu, P. L.; Nakanishi, K.; Woody, R. W. *Comprehensive Chiroptical Spectroscopy, Applications in Stereochemical Analysis of Synthetic Compounds, Natural Products and Biomolecules*; Wiley: New Jersey, 2012; *Vol. 2*.

(9) Tobias, F.; Keiderling, T. A. Role of Side Chains in β-Sheet Self-Assembly into Peptide Fibrils. IR and VCD Spectroscopic Studies of Glutamic Acid-Containing Peptides. *Langmuir* **2016**, *32*, 4653−4661.

(10) Ma, S.; Cao, X.; Mak, M.; Sadik, A.; Walkner, C.; Freedman, T. B.; Lednev, I. K.; Dukor, R. K.; Nafie, L. A. Vibrational Circular Dichroism Shows Unusual Sensitivity to Protein Fibril Formation and Development in Solution. *J. Am. Chem. Soc.* **2007**, *129*, 12364−12365.

(11) Kurouski, D.; Lombardi, R. A.; Dukor, R. K.; Lednev, I. K.; Nafie, L. A. Direct observation and pH control of reversed supramolecular chirality in insulin fibrils by vibrational circular dichroism. *Chem. Commun.* **2010**, *46*, 7154−7156.

(12) Kurouski, D.; Kar, K.; Wetzel, R.; Dukor, R. K.; Lednev, I. K.; Nafie, L. A. Levels of supramolecular chirality of polyglutamine aggregates revealed by vibrational circular dichroism. *FEBS Lett.* **2013**, *587*, 1638−1643.

(13) Kurouski, D.; Lu, X.; Popova, L.; Wan, W.; Shanmugasundaram, M.; Stubbs, G.; Dukor, R. K.; Lednev, I. K.; Nafie, L. A. Is Supramolecular Filament Chirality the Underlying Cause of Major Morphology Differences in Amyloid Fibrils? *J. Am. Chem. Soc.* **2014**, *136*, 2302−2312.

(14) Fulara, A.; Lakhani, A.; Wójcik, S.; Nieznańska, H.; Keiderling, T. A.; Dzwolak, W. Spiral Superstructures of Amyloid-Like Fibrils of Polyglutamic Acid: An Infrared Absorption and Vibrational Circular Dichroism Study. *J. Phys. Chem. B* **2011**, *115*, 11010−11016.

(15) Chi, H.; Welch, W. R. W.; Kubelka, J.; Keiderling, T. A. Insight into the Packing Pattern of β2 Fibrils: A Model Study of Glutamic Acid Rich Oligomers with 13C Isotopic Edited Vibrational Spectroscopy. *Biomacromolecules* **2013**, *14*, 3880−3891.

(16) Welch, W. R. W.; Keiderling, T. A.; Kubelka, J. Structural Analyses of Experimental 13C Edited Amide I′ IR and VCD for Peptide β-Sheet Aggregates and Fibrils Using DFT-Based Spectral Simulations. *J. Phys. Chem. B* **2013**, *117*, 10359−10369.

(17) Kessler, J.; Keiderling, T. A.; Bouř, P. Arrangement of Fibril Side Chains Studied by Molecular Dynamics and Simulated Infrared and Vibrational Circular Dichroism Spectra. *J. Phys. Chem. B* **2014**, *118*, 6937−6945.

(18) Yamamoto, S.; Watarai, H. Raman Optical Activity Study on Insulin Amyloid and Prefibril Intermediate. *Chirality* **2011**, *24*, 97−103.

(19) Jungwirth, J. *Application of Chiroptical Techniques for Exploration of Inhomogeneous Systems*; Charles University: Prague, 2017.

(20) Wu, T.; Kapitán, J.; Mašek, V.; Bouř, P. Detection of Circularly Polarized Luminescence of a Cs-Eu^{III} Complex in Raman Optical Activity Experiments. *Angew. Chem., Int. Ed.* **2015**, *54*, 14933−14936.

(21) Binnemans, K. Interpretation of europium(III) spectra. *Coord. Chem. Rev.* **2015**, *295*, 1−45.

(22) Walrand, C. G.; Binnemans, K. Rationalization of Crystal-Field Parametrization. In *Handbook on the Physics and Chemistry of Rare Earths*; Gschneider, K. A., Eyring, L., Eds.; Elsevier Science B. V.: Amsterdam, 1996; pp 121−283.

DOI: 10.1021/acsomega.8b03175
ACS Omega 2019, 4, 1265−1271

(23) Brichtová, E.; Hudecová, J.; Vršková, N.; Šebestík, J.; Bouř, P.; Wu, T. Binding of Lanthanide Complexes to Histidine-Containing Peptides Probed by Raman Optical Activity Spectroscopy. *Chem.—Eur. J.* **2018**, *24*, 8664−8669.
(24) Wu, T.; Průša, J.; Kessler, J.; Dračínský, M.; Valenta, J.; Bouř, P. Detection of Sugars via Chirality Induced in Europium(III) Compounds. *Anal. Chem.* **2016**, *88*, 8878−8885.
(25) Wu, T.; Kessler, J.; Bouř, P. Chiral sensing of amino acids and proteins chelating with EuIII complexes by Raman optical activity spectroscopy. *Phys. Chem. Chem. Phys.* **2016**, *18*, 23803−23811.
(26) Rybicka, A.; Longhi, G.; Castiglioni, E.; Abbate, S.; Dzwolak, W.; Babenko, V.; Pecul, M. Thioflavin T: Electronic Circular Dichroism and Circularly Polarized Luminescence Induced by Amyloid Fibrils. *ChemPhysChem* **2016**, *17*, 2931−2937.
(27) Xue, C.; Lin, T. Y.; Chang, D.; Guo, Z. Thioflavin T as an amyloid dye: fibril quantification, optimal concentration and effect on aggregation. *R. Soc. Open Sci.* **2017**, *4*, 160696.
(28) Barron, L. D. *Molecular Light Scattering and Optical Activity*; Cambridge University Press: Cambridge, U.K., 2004.
(29) Wu, T.; Kessler, J.; Kaminský, J.; Bouř, P. Recognition of Oligosaccharides by Chirality Induced in Europium (III) Compounds. *Chem.−Asian J.* **2018**, *13*, 3865−3870.
(30) Zinna, F.; Resta, C.; Abbate, S.; Castiglioni, E.; Longhi, G.; Mineo, P.; Di Bari, L. Circularly polarized luminescence under near-UV excitation and structural elucidation of a Eu complex. *Chem. Commun.* **2015**, *51*, 11903−11906.
(31) Keith, H. D.; Giannoni, G.; Padden, F. J. Single crystal of poly(L-glutamic acid). *Biopolymers* **1969**, *7*, 775−792.
(32) Itoh, K.; Foxman, B. M.; Fasman, G. D. The two β forms of poly(L-glutamic acid). *Biopolymers* **1976**, *15*, 419−455.
(33) Yamaoki, Y.; Imamura, H.; Fulara, A.; Wójcik, S.; Bożycki, Ł.; Kato, M.; Keiderling, T. A.; Dzwolak, W. An FT-IR Study on Packing Defects in Mixed β-Aggregates of Poly(Lglutamic acid) and Poly(D-glutamic acid): A High-Pressure Rescue from a Kinetic Trap. *J. Phys. Chem. B* **2012**, *116*, 5172−5178.
(34) Vijay, R.; Polavarapu, P. L. Molecular Structural Transformations Induced by Spatial Confinement in Barium Fluoride Cells. *J. Phys. Chem. A* **2013**, *117*, 14086−14094.
(35) Průša, J.; Bouř, P. Transition dipole coupling modeling of optical activity enhancements in macromolecular protein systems. *Chirality* **2017**, *30*, 55−64.
(36) Weiss, M. S.; Palm, G. J.; Hilgenfeld, R. Crystallization, structure solution and refinement of hen egg-white lysozyme at pH 8.0 in the presence of MPD. *Acta Crystallogr., Sect. D: Biol. Crystallogr.* **2000**, *56*, 952−958.
(37) Job, P. Formation and Stability of Inorganic Complexes in Solution. *Ann. Chim. Appl.* **1928**, *9*, 113−203.
(38) Andrushchenko, V.; Bouř, P. Circular Dichroism Enhancement in Large DNA Aggregates Simulated by a Generalized Oscillator Model. *J. Comput. Chem.* **2008**, *29*, 2693−2703.
(39) Li, H.; Nafie, L. A. Simultaneous acquisition of all four forms of circular polarization Raman optical activity: results for α-pinene and lysozyme. *J. Raman Spectrosc.* **2011**, *43*, 89−94.
(40) Castiglioni, E.; Abbate, S.; Lebon, F.; Longhi, G. Chiroptical spectroscopic techniques based on fluorescence. *Methods Appl. Fluoresc.* **2014**, *2*, 024006.
(41) Wu, T.; Kapitán, J.; Andrushchenko, V.; Bouř, P. Identification of Lanthanide(III) Luminophores in Magnetic Circularly Polarized Luminescence Using Raman Optical Activity Instrumentation. *Anal. Chem.* **2017**, *89*, 5043−5049.
(42) Turner, D. H.; Tinoco, I.; Maestre, M. Fluorescence detected circular dichroism. *J. Am. Chem. Soc.* **1974**, *96*, 4340−4342.
(43) Kapitán, J.; Barron, L. D.; Hecht, L. A novel Raman optical activity instrument operating in the deep ultraviolet spectral region. *J. Raman Spectrosc.* **2015**, *46*, 392−399.
(44) Haraguchi, S.; Shingae, T.; Fujisawa, T.; Kasai, N.; Kumauchi, M.; Hanamoto, T.; Hoff, W. D.; Unno, M. Spectroscopic ruler for measuring active-site distortions based on Raman optical activity of a hydrogen out-of-plane vibration. *Proc. Natl. Acad. Sci. U.S.A.* **2018**, *115*, 8671−8675.
(45) Zhang, Y.; Wang, P.; Jia, G.; Cheng, F.; Feng, Z.; Li, C. A Short-Wavelength Raman Optical Activity Spectrometer with Laser Source at 457nm for the Characterization of Chiral Molecules. *Appl. Spectrosc.* **2017**, *71*, 2211−2217.
(46) Fulara, A.; Dzwolak, W. Bifurcated Hydrogen Bonds Stabilize Fibrils of Poly(L-glutamic) Acid. *J. Phys. Chem. B* **2010**, *114*, 8278−8283.
(47) Hug, W.; Hangartner, G. A novel high-throughput Raman spectrometer for polarization difference measurements. *J. Raman Spectrosc.* **1999**, *30*, 841−852.
(48) Nafie, L. A. Vibrational optical activity. *Appl. Spectrosc.* **1996**, *50*, 14A−26A.
(49) Hug, W. Virtual enantiomers as the solution of optical activity's deterministic offset problem. *Appl. Spectrosc.* **2003**, *57*, 1−13.

DOI: 10.1021/acsomega.8b03175
ACS Omega 2019, 4, 1265−1271